# Stability of Taylor-Dean flow in an annulus with arbitrary gap spacing

Falin Chen
*Institute of Applied Mechanics, National Taiwan University, Taipei, Taiwan 10764, Republic of China*
(Received 18 February 1992; revised manuscript received 19 June 1992)

A linear stability analysis based on three-dimensional disturbances is implemented for the Taylor-Dean flow, a viscous flow driven simultaneously by a rotating inner cylinder and an azimuthal pressure gradient within an annulus with an arbitrary gap spacing. It is found that nonaxisymmetric instability modes prevail for a wide variety of basic flows. The most stable state is always associated with the smallest critical axial wavelength as well as with the onset of instability being largely confined to a small portion within the gap. The flow reaches the most stable state either when the corresponding instability is about to change from a nonaxisymmetric mode into an axisymmetric mode, as the pumping velocity is increasing, or when a nonaxisymmetric mode changes both its azimuthal wavelength and its direction of traveling. The nonaxisymmetric mode with smaller azimuthal wave number becomes increasingly significant as the gap increases in width. From both the present calculated results and previous experimental observations, it is inferred that nonlinear interactions between different instability modes may occur when the basic flow is near the most stable state.

PACS number(s): 47.20.−k, 47.32.−y

## I. INTRODUCTION

The Taylor-Dean problem is concerned with the stability of a viscous flow between two concentric cylinders, in which the basic flow (referred to as the Taylor-Dean flow) is the combination of a circular Couette flow (Taylor problem [1]) and an azimuthal Poiseuille flow (Dean problem [2]). The stability of the Taylor-Dean flow is of both academic and engineering application interest. In engineering applications, the flow driven by both rotating cylinders and an azimuthal pressure gradient can be found in, for example, an electrogalvanizing line in the steel-making industry, which uses a roller-type cell to plate zinc onto the surface of a steel strip [3,4], and in a rotating drum filter used in the paper and the board-making industry, in which a sheet of fiber is taken off from a drum rotating in a vat full of fiber suspensions [5]. Engineers in the paper industry had observed that longitudinal streaks regularly spaced along the axis of the drum arise in the formed sheet, an obvious result of the secondary fluid motion predominating in the curved passage. In view of the fundamental interest in the flow pattern formation and the transition sequence from steady basic state to disorders, Mutabazi *et al.* [6,7] conducted a series of experiments in a system consisting of two horizontal coaxial rotating cylinders with a partially filled gap. In such a system, they found some sort of traveling waves prevailing in the supercritical regime. Chen *et al.* [8] conducted both experimental and computational studies to investigate the radial distribution of azimuthal velocity of basic flow within an exactly-half-filled gap.

The Taylor-Dean problem was first studied experimentally by Brewster and Nissan [5] and both experimentally and theoretically by Brewster, Grosberg, and Nissan [9]. The small-gap approximation was assumed in their theoretical analyses. Later, the theoretical analysis was extended by DiPrima [10], who used the Fourier expansion technique to study the problem with small-gap approximation in a larger range of $\beta$ (a parameter that characterizes the ratio of average pumping velocity to the rotating velocity due to inner cylinder rotation), and by Meister [11], as well as Sparrow and Lin [12], who employed a shooting technique to attack the problem of arbitrary gap spacings. All these studies considered the onset of instability to be axisymmetric as well as stationary and were restricted to the case of $\mu=0$, in which the inner cylinder is rotating while the outer cylinder is fixed. Note that $\mu=\Omega_2/\Omega_1$, where $\Omega_1$ and $\Omega_2$ are angular velocities of inner and outer cylinders, respectively.

Of particular interest is the result obtained by DiPrima [10] that the flow is most stable near $\beta=-3.5$, at which the critical wave number ($a^c$) jumps discontinuously from 5.8 to 7.4 as $\beta$ decreases. Kruzweg [13] showed analytically that the larger $a^c$ corresponds to the instability occurring in the region near the inner cylinder and the smaller $a^c$ is related to the instability confined to the region near the outer cylinder. Hughes and Reid [14] found that the discontinuity of $a^c$ corresponds to the fact that the neutral curve consists of two separated branches. They also pointed out that the jump of $a^c$ occurs precisely at $\beta^*=-3.667$. Raney and Chang [15] showed that there exists an oscillatory axisymmetric mode of approximately equal stability with that of the steady mode in the vicinity of $\beta^*$. They also indicated that, although the resulting reduction of the value of the critical Taylor number $T^c$ is not significant, the most critical mode is oscillatory nonaxisymmetric with $m=1$ in $-3.850<\beta<-3.635$, where $m$ is the azimuthal wave number. Later, the topology of neutral curves was extensively studied by Kachoyan [16] for the axisymmetric mode.

An azimuthally fully developed Taylor-Dean flow in an annulus seems to be an artificial case since, under any circumstance, to provide an external pressure gradient in

 

the azimuthal direction there must be an associated breakdown of the symmetry of the geometry of the annulus, which makes a fully developed basic flow impossible. Nevertheless, the Taylor-Dean flow may exist in a portion of the annulus, such as the flow in eccentric rotating cylinders [17] or the flow in a partially filled horizontal annulus [8,18]. Mutabazi *et al.* [6,7] implemented an experimental investigation for the Taylor-Dean flow in the latter configuration, in which the flow consists of a core region with a Taylor-Dean basic flow and two recirculation zones adjacent to free surfaces. Later, Mutabazi *et al.* [19] analyzed the linear stability of the Taylor-Dean flow of the core region. For the partially filled horizontal annulus case, the average velocity due to the rotating cylinders is equal to, but opposite in direction to, the average velocity due to the pressure gradient caused by the free surface within the gap; namely, $\beta=-3$. In the analysis of Mutabazi *et al.* [19], the small-gap approximation was made and the cases for $\mu\geq 0$ were considered. Their analysis resulted in a larger critical Taylor number compared with the corresponding experimental results [6]. They also found that the nonaxisymmetric instability modes prevail in the range $0.29\leq\mu\leq 0.61$. To study the flow pattern formation as well as the transition from the basic state to disorder, Mutabazi and coworkers [6,7,20] conducted a series of experiments for a variety of $\mu$ in the same configuration. They indicated that some sort of nonlinear interaction, such as spatiotemporal pattern modulation, may exist in the Taylor-Dean flow.

Recently, in a three-dimensional liner stability analysis of the small-gap problem, Chen and Chang [21] showed that nonaxisymmetric instability modes prevail in wide ranges of both $\beta$ and $\mu$. In particular, the peculiar neutral curve of $m=0$ for $\beta^*=-3.667$ is found to be replaced by the neutral curve of $m=5$, which is unimodal and the most unstable. Furthermore, they indicated, in general, that the instability mode with a larger $m$ is of greater stability and smaller critical axial wavelength, the most stable state occurring at a $\beta$ on which the azimuthal traveling wave changes its direction. In comparison with the result of Mutabazi *et al.* [19] for the case of $\beta=-3$, Chen and Chang [21] ended up with that the nonaxisymmetric mode instability predominates in the system in the range $\mu\leq 0.35$, which is much larger than that of Mutabazi *et al.* [19]. This discrepancy will be discussed in Sec. III E.

In the present study, we extend the analysis of Chen and Chang [21] by lifting the small-gap assumption. We first compare the calculated results with those of previous studies. A systematic parameter study covering wide ranges of $\eta$ and $\beta$ is then conducted. To reduce the parametric space, only the case of $\mu=0$ will be considered. The general stability characteristics and the nature of the nonaxisymmetric modes, as well as the corresponding traveling waves in the azimuthal direction, are discussed. A comparison between present results and previous experimental and theoretical findings is also provided. A general conclusion reached by the present study is that the consideration of three-dimensional perturbations in a stability analysis of Taylor-Dean flow is essential.

## II. PROBLEM FORMULATION AND METHOD OF SOLUTION

We consider two infinitely long concentric circular cylinders with the $z$ axis as their common axis, and let $R_1$ and $R_2$ denote the radii of inner and outer cylinders, respectively. The flow in the annulus is driven simultaneously by the rotating inner cylinder and by an azimuthal pressure gradient. A cylindrical coordinate system is chosen that is usually denoted by $r$, $\theta$, and $z$. If $U_r$, $U_\theta$, and $U_z$ are the velocity components in the increasing $r$, $\theta$, and $z$ directions, the Navier-Stokes equations admit a steady solution in terms of velocities of three components

$$U_r=U_z=0\ ,\quad U_\theta=V(r)\ . \tag{1}$$

The basic-state velocity $V(r)$, a combination of the fully developed velocity distributions of circular Couette and azimuthal Poiseuille flows, is described by

$$V(r)=Ar+B/r+\frac{1}{2\rho\nu}\frac{\partial P}{\partial\theta}(r\ln r+Cr+E/r)\ , \tag{2}$$

where $\rho$, $\nu$, and $P$ are density, kinematic viscosity of the fluid, and pressure of the basic flow, respectively. The constants are

$$\begin{aligned} &A=\Omega_1\frac{\mu-\eta^2}{1-\eta^2}\ ,\quad B=\Omega_1 R_2^2\eta^2\frac{1-\mu}{1-\eta^2}\ ,\\ &C=-\frac{\ln R_2-\eta^2\ln R_1}{1-\eta^2}\ ,\quad E=-\frac{R_1^2}{1-\eta^2}\ln\eta\ . \end{aligned} \tag{3}$$

The $\partial P/\partial\theta$ in (2) accounts for the basic-state azimuthal pressure gradient due to external pumping, and $\eta$ is the ratio of radii $R_1/R_2$. Note that the pressure may not be single valued, i.e., $P(\theta+2\pi)\neq P(\theta)$, if free surfaces are present.

To study the stability of this flow, we superimpose a general disturbance on the basic solution

$$\mathbf{u}=(u_r,V(r)+u_\theta,u_z)\ ,\quad \Pi=P+p\ , \tag{4}$$

where $u_r$, $u_\theta$, $u_z$, and $p$ are the three components of the small-disturbance velocity and pressure, respectively. We then substitute (4) into the equations of motion and the continuity equation and neglect quadratic terms, and yield

$$\frac{\partial u_r}{\partial r}+\frac{u_r}{r}+\frac{1}{r}\frac{\partial u_\theta}{\partial\theta}+\frac{\partial u_z}{\partial z}=0\ , \tag{5}$$

$$\begin{aligned} &\frac{\partial u_r}{\partial t}+\frac{V}{r}\frac{\partial u_r}{\partial\theta}-\frac{2Vu_\theta}{r}\\ &\qquad=-\frac{1}{\rho}\frac{\partial p}{\partial r}+\nu\left[\nabla^2 u_r-\frac{u_r}{r^2}-\frac{2}{r^2}\frac{\partial u_\theta}{\partial\theta}\right]\ , \end{aligned} \tag{6}$$

$$\begin{aligned} &\frac{\partial u_\theta}{\partial t}+\frac{V}{r}\frac{\partial u_\theta}{\partial\theta}+(D_* V)u_r\\ &\qquad=-\frac{1}{\rho}\frac{1}{r}\frac{\partial p}{\partial\theta}+\nu\left[\nabla^2 u_\theta-\frac{u_\theta}{r^2}+\frac{2}{r^2}\frac{\partial u_r}{\partial\theta}\right]\ , \end{aligned} \tag{7}$$

$$\frac{\partial u_z}{\partial t}+\frac{V}{r}\frac{\partial u_z}{\partial\theta}=-\frac{1}{\rho}\frac{\partial p}{\partial z}+\nu\nabla^2 u_z\ , \tag{8}$$

where

$$\nabla^2=\frac{\partial^2}{\partial r^2}+\frac{1}{r}\frac{\partial}{\partial r}+\frac{1}{r^2}\frac{\partial^2}{\partial\theta^2}+\frac{\partial^2}{\partial z^2}$$

and

$$D_*=\frac{d}{dr}+\frac{1}{r}\ .$$

We then employ the normal-mode analysis for the small-disturbance quantities

$$(u_r,u_\theta,u_z)=\delta\Omega_1(u(r),v(r),w(r))\exp[i(st+m\theta+\lambda z)] \tag{9}$$

and

$$p=\rho\nu\Omega_1\pi(r)\exp[i(st+m\theta+\lambda z)]\ , \tag{10}$$

where $\lambda$ is the axial wave number and $m$ is the azimuthal wave number, which are, in general, real. For the sake of finite resources of computing, we consider only the integer values of $m$ in this study. It turns out, as will be seen in Sec. III, the growth rates of the instability appear to be fairly smooth functions of $m$ and thus the instability mode with noninteger values of $m$ can be inferred by interpolation. The parameter $s$ is, in general, complex and $\delta=R_2-R_1$.

We now introduce the dimensionless variables

$$\begin{aligned} &r=R_1+x\delta\ ,\quad \Delta=\delta/R_1,\quad a=\lambda\delta\ ,\quad \sigma=s\delta^2/\nu\ ,\\ &k=(-\Omega_1/4A)^{1/2}m\ ,\quad T=-4A\Omega_1\delta^4/\nu^2\ . \end{aligned} \tag{11}$$

After substituting (9) and (10) into (5)–(8) and introducing

$$\begin{aligned} &\pi(x)=D'_*u(x)-X(x)\ ,\quad Y(x)=D'_*v(x)\ ,\\ &Z(x)=D'w(x)\ , \end{aligned} \tag{12}$$

where

$$D'=\frac{d}{dx}\ ,\quad D'_*=\frac{d}{dx}+\xi(x)\ ,\quad \xi(x)=\frac{\Delta}{1+\Delta x}\ , \tag{13}$$

we obtain

$$D'_*u(x)=-im\xi(x)v(x)-iaw(x)\ , \tag{14}$$

$$\begin{aligned} D'X(x)=&\left[i\sigma+im\delta^2\frac{V}{r\nu}+\xi^2(x)m^2+a^2\right]u(x)\\ &+2\left[im\xi^2(x)-\frac{V\delta^2}{r\nu}\right]v(x)\ , \end{aligned} \tag{15}$$

$$\begin{aligned} D'Y(x)=&\left[\frac{is\delta^2}{\nu}+im\delta^2\frac{V}{r\nu}+2m^2\xi^2(x)+a^2\right]v(x)\\ &+ma\xi(x)w(x)-im\xi(x)X(x)\\ &+\left[\frac{d^2}{\nu}D_*V-2im\xi^2(x)\right]u(x)\ , \end{aligned} \tag{16}$$

$$\begin{aligned} D'_*Z(x)=&\left[\frac{is\delta^2}{\nu}+im\delta^2\frac{V}{r\nu}+m^2\xi^2(x)+a^2\right]w(x)\\ &-iaX(x)+am\xi(x)v(x)+a^2w(x)\ . \end{aligned} \tag{17}$$

In these equations, the basic velocity, $V$, as shown in (2), can be rewritten as

$$V(x)=r\Omega_1\left[g(x)+\frac{\beta h(x)\xi(x)}{6\Delta}\right]\ , \tag{18}$$

in which

$$g(x)=\frac{A}{\Omega_1}+\frac{B}{\Omega_1 r_1^2\delta^2}\xi^2(x) \tag{19}$$

and

$$\begin{aligned} h(x)=&\frac{4(1-\eta)}{4\eta^2(\ln\eta)^2-(1-\eta^2)^2}\eta\Delta\frac{1}{\xi(x)}\\ &\times\left\{(1-\eta^2)\ln\left[\frac{\eta\Delta}{\xi(x)}\right]+\eta^2\ln\eta\left[1-\frac{\xi^2(x)}{\eta^2\Delta^2}\right]\right\}\ . \end{aligned} \tag{20}$$

The parameter $\beta$, which in essence accounts for the ratio of average pumping velocity to rotating velocity, is defined as

$$\beta=\frac{6V_m}{\Omega_1R_1}\ , \tag{21}$$

where $V_m$ is the average pumping velocity

$$\begin{aligned} V_m=&\frac{1}{\Delta}\int_{R_1}^{R_2}\frac{1}{2\rho\nu}\frac{\partial P}{\partial\theta}(r\ln r+Cr+E/r)dr\\ =&\frac{-R_2}{2\rho\nu}\frac{\partial P}{\partial\theta}\frac{(1-\eta^2)^2-4\eta^2(\ln\eta)^2}{4(1-\eta)(1-\eta^2)}\ . \end{aligned} \tag{22}$$

By substituting (18) into (14)–(17) and making some rearrangement, one yields the final equations

$$D'X(x)=M(x)u(x)+2[im\xi^2(x)-\tfrac{1}{2}\sqrt{T}K(x)]v(x)\ , \tag{23}$$

$$\begin{aligned} D'Y(x)=&[M(x)+m^2\xi^2(x)]v(x)+ma\xi(x)w(x)\\ &-im\xi(x)X(x)\\ &+\left\{\frac{-\sqrt{T}}{n}\left[1+\frac{\beta\Omega_1}{12A\Delta}D'_*h(x)\right]\right.\\ &\left.-2im\xi^2(x)\right\}u(x)\ , \end{aligned} \tag{24}$$

$$\begin{aligned} D'Z(x)=&[M(x)+a^2]w(x)-iaX(x)\\ &+[amv(x)-Z(x)]\xi(x)\ , \end{aligned} \tag{25}$$

where $n=(-A/\Omega_1)^{-1/2}$ and

$$K(x)=\left[g(x)+\frac{\beta h(x)\xi(x)}{6\Delta}\right]\ ,$$

and

$$M(x)=a^2+m^2\xi^2(x)+i[\sigma+\tfrac{1}{2}mn\sqrt{T}K(x)] .$$

We rewrite (12) and (14) into the following

$$D'u(x)=-[imv(x)+u(x)]\xi(x)-iaw(x) , \quad (26)$$

$$D'v(x)=Y(x)-\xi(x)v(x) , \quad (27)$$

$$D'w(x)=Z(x) . \quad (28)$$

The relevant boundary conditions are

$$u(x)=v(x)=w(x)=0 \quad \text{at } x=0,1 . \quad (29)$$

Note that (23)–(28) can be reduced into Eq. (21) of Krueger, Gross, and DiPrima [22] for the wide-gap Taylor problem if $\beta=0$ is assumed. They can also become the governing equations for either the wide-gap or the small-gap Taylor-Dean problem for axisymmetric disturbance, as shown in, for example, Sparrow and Lin [12] and DiPrima [10], respectively, if proper assumptions are imposed.

The ordinary differential equations (ODE's) (23)–(28) with the boundary conditions (29) determine an eigenvalue problem of the form

$$F(\eta,\mu,\beta,m,a,\sigma,T)=0 . \quad (30)$$

The marginal state is characterized by $\sigma_i$, the imaginary part of $\sigma$, equal to zero. For given values of $\eta$, $\mu$, and $\beta$, we seek the minimum real positive $T$ over real $a>0$ and integer $m\geq 0$, for which there is a solution for (30) with $\sigma_i=0$. The sought value of $T$ is the critical Taylor number $T^c$ for assigned values of $\eta$, $\mu$, and $\beta$. The values of $a$ and $m$ corresponding to $T^c$ determine the form of the critical disturbance. Moreover, the real part of $\sigma$, namely $\sigma_r$, corresponding to $T^c$, determines the frequency of the oscillation as well as the angular velocity of the traveling wave. We solve the two-point eigenvalue problem defined by (23)–(29) with a shooting technique together with a unit-disturbance method. This method has been used by, for example, DiPrima [23], Harris and Reid [24], Sparrow, Munro, and Jonsson [25], and Krueger, Gross, and DiPrima [22], for similar hydrodynamic stability problems, and more recently, by Chen and Chang [21] for the small-gap Taylor-Dean problem. For details of the computational procedure, the reader is referred to Krueger, Gross, and DiPrima [22].

Once the eigenvalues $T^c$ and $\sigma_r$ are obtained, the eigenfunctions of $u$, $v$, and $w$, which during the integration are considered complex as $u(r)=u_r(r)+iu_i(r)$, $v(r)=v_r(r)+iv_i(r)$, and $w(r)=w_r(r)+iw_i(r)$, respectively, can be determined by another direct integration. One then substitutes the eigenfunction into the relation (9) and takes the real part to yield the function of small-disturbance velocity,

$$\psi(r,\theta,z,t)=u_r(r)\cos(\sigma_r t+m\theta+\lambda z) - u_i(r)\sin(\sigma_r t+m\theta+\lambda z) , \quad (31)$$

$$\phi(r,\theta,z,t)=v_r(r)\cos(\sigma_r t+m\theta+\lambda z) - v_i(r)\sin(\sigma_r t+m\theta+\lambda z) , \quad (32)$$

$$\chi(r,\theta,z,t)=w_r(r)\cos(\sigma_r t+m\theta+\lambda z) - w_i(r)\sin(\sigma_r t+m\theta+\lambda z) . \quad (33)$$

## III. RESULTS AND DISCUSSION

In this study, we consider $\mu=0$ where the inner cylinder is rotating while the outer cylinder is stationary. The analysis covers wide ranges of $\eta$ and $\beta$. We first, in Sec. III A, check our computer code by considering the special case $\beta=0$, which is equivalent to the Taylor problem as considered in Krueger, Gross, and DiPrima [22]. Then the significance of the gap width to the stability characteristics of Taylor-Dean flow is examined in Sec. III B by comparing the results of $\eta=0.95$ to those of $\eta\approx 1$ [21]. A discussion of the general stability characteristics is provided in Sec. III C, in which a detailed description of the prevalence of the nonaxisymmetric modes and the corresponding stability features is provided. In Sec. III D, the nature of the neutral curves is illustrated, from which possible nonlinear interactions between different instability modes at the supercritical stage are discussed. Finally, in Sec. III E, we compare the present results with some of previous investigations.

### A. The case of $\beta=0$: The Taylor problem

For $\beta=0$, the azimuthal pressure gradient vanishes, and the Taylor-Dean formulation is reduced to the Taylor formulation. For the purpose of verification of our

TABLE I. Comparison between the results of the present study for $\beta=0$ ($A$) and those of Krueger, Gross, and DiPrima [22] ($B$).

| | | | $a^c$ | | $T^c$ | | $-\sigma$ | |
|---|---|---|---|---|---|---|---|---|
| $\eta$ | $\mu$ | $m$ | $A$ | $B$ | $A$ | $B$ | $A$ | $B$ |
| 0.95 | 0.0 | 0 | 3.128 | 3.128 | 3509.7 | 3509.9 | 0 | 0 |
| | −0.8 | 3 | 3.56 | 3.561 | 13 728 | 13 730 | 15.1371 | 15.106 |
| | −1.0 | 4 | 3.68 | 3.680 | 20 068 | 20 072 | 23.3823 | 23.358 |
| | −1.5 | 6 | 4.00 | 4.002 | 45 290 | 45 307 | 43.6146 | 43.616 |
| | −2.0 | 7 | 4.49 | 4.483 | 91 235 | 91 298 | 64.2612 | 64.147 |
| 0.9 | −1.0 | 3 | 3.72 | 3.721 | 23 855 | 23 861 | 26.8755 | 26.896 |
| 0.8 | −1.0 | 2 | 3.84 | 3.835 | 36 751 | 36 767 | 32.9800 | 33.009 |
| 0.7 | −1.0 | 2 | 3.99 | 3.984 | 60 065 | 60 099 | 48.5117 | 48.472 |
| 0.6 | −1.0 | 2 | 4.46 | 4.456 | 113 960 | 114 043 | 72.8252 | 72.626 |

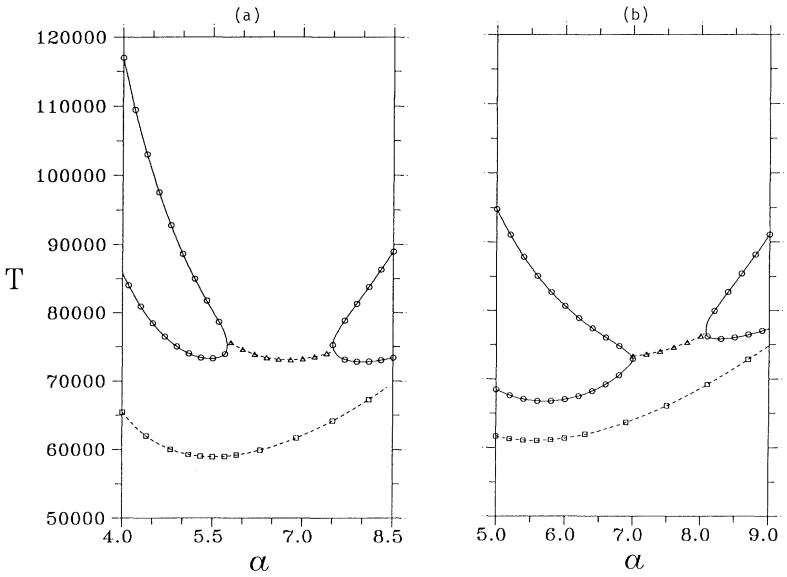


FIG. 1. Neutral curves for $\eta=0.95$ and various $\beta$. —○—: axisymmetric stationary mode $m=0$; - - -Δ- - -: axisymmetric oscillatory mode $m=0$; - - -□- - -: nonaxisymmetric mode $m=6$. (a) $\beta=-3.65$; (b) $\beta=-3.7$.

numerical results, we recompute the cases considered in Krueger, Gross, and DiPrima [22] by using our computer code. One can see in Table I that the comparison results in excellent agreement.

### B. Significance of the gap width

In this section, we consider the case of $\eta=0.95$, which can be compared with the small-gap case [21] $\eta\approx 1$. In the case $\eta\approx 1$ and $\beta\sim\beta^*=-3.667$, the neutral curve in terms of $T$ versus $a$ consists of two separated curves for the stationary axisymmetric mode [10,14] and one connecting curve lying between these two branches for the oscillatory axisymmetric mode [15]. In considering the instability against three-dimensional disturbances, Chen and Chang [21] found that the most unstable mode for $\beta\sim\beta^*$ is nonaxisymmetric with $m=5$, which is an instability mode with five waves traveling in the azimuthal direction. For the wide-gap case with $\eta=0.95$ (Fig. 1), we find that the neutral curves for the axisymmetric mode are similar to those of the small-gap case, while the most unstable mode is nonaxisymmetric with $m=6$.

In Table II, the comparison between the results of $\eta=0.95$ and $\eta\approx 1$ in terms of $T^c$, $a^c$, $m$, and $\sigma$ for $-10\le\beta\le 10$ is made. It is found, by and large, that the flow of $\eta=0.95$ is slightly more stable than that of $\eta\approx 1$,

TABLE II. Comparison between results of the wide-gap problem of $\eta=0.95$ ($A$) and those of the small-gap problem of $\eta\approx 1$ ($B$) [21].

| | $m$ | | $a^c$ | | $T^c$ | | $\sigma$ | |
|---|---|---|---|---|---|---|---|---|
| $\beta$ | $A$ | $B$ | $A$ | $B$ | $A$ | $B$ | $A$ | $B$ |
| 10.0 | 0 | 0 | 3.49 | 3.46 | 481 | 454 | 0 | 0 |
| 5.0 | 0 | 0 | 3.25 | 3.24 | 1049 | 992 | 0 | 0 |
| 0.0 | 0 | 0 | 3.13 | 3.13 | 3510 | 3390 | 0 | 0 |
| −1.0 | 0 | 0 | 3.24 | 3.23 | 5587 | 5417 | 0 | 0 |
| −2.0 | 0 | 0 | 3.82 | 3.79 | 13016 | 12540 | 0 | 0 |
| −2.1 | | 0 | | 3.96 | | 14166 | | 0 |
| −2.15 | 1 | | 4.10 | | 15692 | | −6.6221 | |
| −2.2 | 2 | 1 | 4.15 | 4.14 | 16663 | 16076 | −13.7162 | −5.5416 |
| −2.3 | 3 | 2 | 4.22 | 4.24 | 18575 | 18021 | −21.7815 | −12.0343 |
| −2.4 | | 3 | | 4.28 | | 19916 | | −18.7197 |
| −3.0 | 4 | 4 | 4.76 | 4.72 | 34988 | 33910 | −43.1750 | −34.4285 |
| −3.6 | 5 | | 5.35 | | 56765 | | −69.6927 | |
| −3.7 | 6 | 5 | 5.56 | 5.44 | 61013 | 59347 | −80.8636 | −59.6907 |
| −3.73 | 6 | 5 | 5.58 | 5.46 | 62303 | 60667 | −81.9674 | −60.9290 |
| −3.75 | 2 | 2 | 5.66 | 5.69 | 61508 | 60729 | 30.2877 | 33.3718 |
| −3.9 | 1 | 2 | 5.59 | 5.61 | 51687 | 50990 | 14.9222 | 32.6147 |
| −4.0 | 1 | 1 | 5.54 | 5.56 | 46276 | 45601 | 14.6621 | 16.1222 |
| −4.1 | 0 | 0 | 5.49 | 5.52 | 41606 | 40962 | 0 | 0 |
| −5.0 | 0 | 0 | 5.17 | 5.18 | 18870 | 18449 | 0 | 0 |
| −10.0 | 0 | 0 | 4.56 | 4.56 | 2078 | 2005 | 0 | 0 |

while the critical axial wavelengths are virtually the same. In addition, the frequency of the nonaxisymmetric mode of $\eta=0.95$ is significantly different from the corresponding one of $\eta\approx 1$. In order words, although the small-gap approximation results in a small difference in terms of $T^c$ and $a^c$ from $\eta=0.95$, the frequency of the instability mode is nevertheless significantly influenced by this zero-curvature assumption.

### C. General stability characteristics

We present in Figs. 2(a) and 2(b) the map on the $\eta$-$\beta$ plane in which the instability modes ranging from $m=0$ to 5 and the contours of constant $T^c$ and $a^c$ are illustrated. The $\eta$-$\beta$ map covering $0.1\le\eta\le 1$ and $-5\le\beta\le 0$ and the resolutions of $\Delta\eta$ and $\Delta\beta$ are up to 0.05 and 0.1, respectively. Accordingly, there are a total of 969 cases of different $(\eta,\beta)$ considered. The case (or point) corresponding to a nonaxisymmetric mode is represented by a particular mark (see the caption of the figure) and the case of the axisymmetric mode is not marked. Note that the results for $\eta=1$ are those obtained by Chen and Chang [21] for the small-gap problem.

From this map, it is found that nonaxisymmetric modes predominate in the domain within $-4\le\beta\le -2.2$ and $0.25\le\eta\le 1$, beyond which the onset of instability is stationary and axisymmetric. It is also found that azimuthal wave number $m$ increases with both increasing $\eta$ and decreasing $\beta$ when $\beta>-3.8$. For $\beta<-3.8$ (below the dash line), the azimuthal wave number $m$ is decreased to either 1 or 2 and, meanwhile, the direction of the traveling wave is opposite to that for $\beta>-3.8$ (see also Table II for $\eta=0.95$ and $\eta\approx 1$). In general, an increase in the gap width results in a reduction of the azimuthal wave number $m$; for $\eta<0.8$, most of the traveling waves are of $m\le 2$, while for $\eta\ge 0.8$, the $m$ ranges from 0 to 5.

Regarding the stability criteria $T^c$ and $a^c$, Fig. 2(a) shows that the maximum $T^c$ occurs along either the lower boundary dividing the nonaxisymmetric and axisymmetric modes or the boundary separating the nonaxisymmetric modes with the opposite traveling-wave direction. Along the same boundary, the $a^c$ is the largest and experiences a dramatic jump as $\beta$ varies. In a physical sense, the Taylor-Dean flow is in the most stable state either when a nonaxisymmetric mode is switching into an axisymmetric mode as $\beta$ decreases or the nonaxisymmetric mode is changing its traveling-wave direction with different $m$.

In view of the influence of $\beta$ and $\eta$ on the stability characteristics, we found that, generally, the flow in larger gap width is of greater stability, and the most stable state is associated with the smallest critical axial wavelength; also, the value of $a^c$ decreases gradually with decreasing $\beta$ in $\beta>0$, experiences a dramatic change in a small range of $\beta$ (which depends on $\eta$), and remains virtually constant for other $\beta$ considered. More specifically, for $\eta=0.9$, for instance, the $T^c$ increases as $\beta$ decreases for $\beta\ge -3.9$ and becomes a monotonically decreasing function of $\beta$ for $\beta\le -3.9$. In $-3.9\le\beta\le -2.2$ (see dotted line), the instability is nonasymmetric. A similar relation is found for $\eta=0.7$ and 0.5, where the range of $\beta$ corresponding to nonaxisymmetric modes lies in $-3.6\le\beta\le -2.2$ and $-3.4\le\beta\le -2.2$, respectively.

To explain physically the occurrence of the sharp maximum of $T^c$ for the small-gap case $\eta\approx 1$, Chandrasekhar [26] argued that the value of $\beta$ associated with maximum $T^c$ should lie in the neighborhood of $\beta=-3$, at which, based on Rayleigh's criterion [27], the layers of stable and

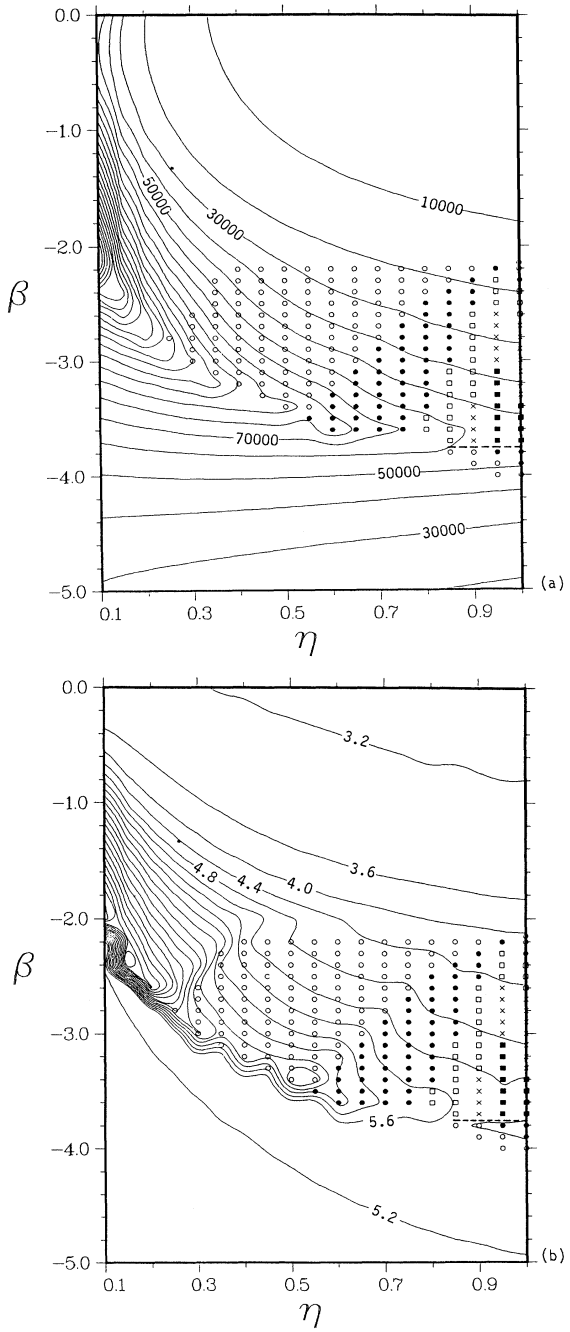


FIG. 2. Map of nonaxisymmetric modes in $\eta$-$\beta$ plane. ---: boundary between the modes with opposite angular velocity. ○: $m=1$; ●: $m=2$; □: $m=3$; ×: $m=4$; ■: $m=5$. (a) Contours of $T^c$, $\Delta T^c=20\,000$; (b) contours of $a^c$, $\Delta a^c=0.4$.

unstable fluid are of equal extent within the gap (see Fig. 94 on p. 356 of Chandrasekhar [26]). When applied to the case of $\mu \neq 0$, however, Hughes and Reid [14] showed that this argument becomes less compelling. Another physical explanation was proposed by DiPrima [10], that the most stable state occurs at $\beta_{\max}$ (was $-3.667$ according to his analysis for the axisymmetric mode) and is due to the fact that, as long as the averaged velocities of pumping and rotation are nearly equal but opposite in sign (note that $\beta=-3$ is the case in which the averaged velocities of pumping and rotation are equal but opposite in direction), they tend to nullify each other before instability thresholds and thus result in a relatively stable state.

To gain physical insights into the maximum $T^c$ for the present problem, which differs from that of Chandrasekhar [26] by considering the viscosity of the fluid and from that of DiPrima [10] by lifting the assumptions of axisymmetric disturbance and small-gap approximation, we present the contours of the small-disturbance velocity in Figs. 3 to 5 for various $\eta$ and $\beta$. For each plot of contours, the abscissa accounts for the axial direction ($z$ direction) and the ordinate for the radial direction ($r$ direction); the width represents half the critical axial wavelength of the perturbed flow and the height is the gap between two cylinders. The contours of three velocity components $\psi$, $\phi$, and $\chi$ can be directly calculated from Eqs. (32), (33), and (34), respectively, in which $t=\theta=0$ is considered, and the perturbation value in each

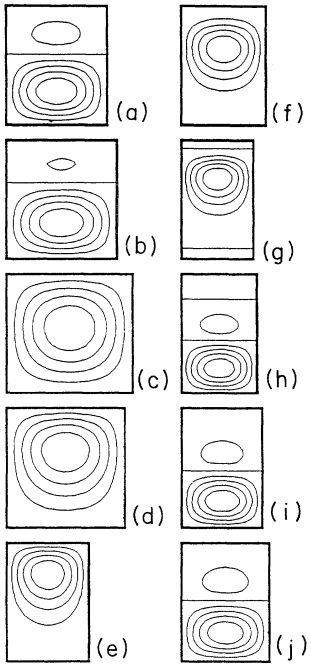


FIG. 4. Contours of $\phi$ of $\eta=0.5$ for various $\beta$. (a) $\beta=10$, $m=0$; (b) $\beta=5$, $m=0$; (c) $\beta=0$, $m=0$; (d) $\beta=-1$, $m=0$; (e) $\beta=-2$, $m=0$; (f) $\beta=-2.2$, $m=1$; (g) $\beta=-2.8$, $m=1$; (h) $\beta=-4$, $m=0$; (i) $\beta=-5$, $m=0$; (j) $\beta=-10$, $m=0$.

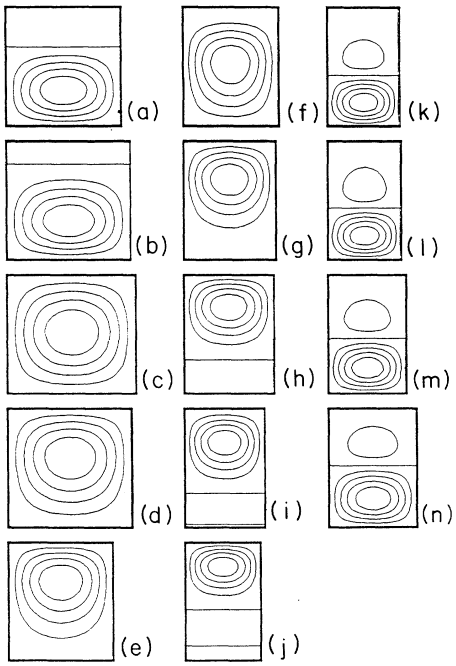


FIG. 3. Contours of $\phi$ of $\eta=0.9$ for various $\beta$. (a) $\beta=10$, $m=0$; (b) $\beta=5$, $m=0$; (c) $\beta=0$, $m=0$; (d) $\beta=-1$, $m=0$; (e) $\beta=-2$, $m=0$; (f) $\beta=-2.2$, $m=1$; (g) $\beta=-2.4$, $m=2$; (h) $\beta=-2.6$, $m=3$; (i) $\beta=-3.2$, $m=3$; (j) $\beta=-3.4$, $m=4$; (k) $\beta=-3.8$, $m=1$; (l) $\beta=-4$, $m=0$; (m) $\beta=-5$, $m=0$; (n) $\beta=-10$, $m=0$.

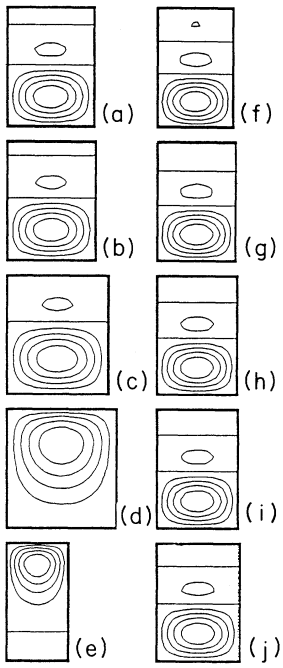


FIG. 5. Contours of $\phi$ of $\eta=0.1$ for various $\beta$. (a) $\beta=10$, $m=0$; (b) $\beta=5$, $m=0$; (c) $\beta=1$, $m=0$; (d) $\beta=-0.4$, $m=0$; (e) $\beta=-1$, $m=0$; (f) $\beta=-2.2$, $m=0$; (g) $\beta=-3$, $m=0$; (h) $\beta=-4$, $m=0$; (i) $\beta=-5$, $m=0$; (j) $\beta=-10$, $m=0$.

case is normalized with respect to its corresponding maximum value (or minimum value if its value is negative). Accordingly, the maximum of the disturbance function in each plot is unity and the contour level is fixed at 0.2.

Note that only the contours of $\phi$ are present since, as concluded from our vast data base, it can stand for the distribution of the onset of instability within the gap. By observing these contours and the associated $T^c$ in Fig. 2(a), one can find that there exist three branches of stability characteristics, in terms of the relation between $T^c$ and $\beta$ as well as the onset flow patterns. The first branch is in the range $\beta > 0$, where $T^c$ increases with decreasing $\beta$ and the onset of instability is confined to the region close to the inner cylinder. The second branch lies within $\beta_{\max} < \beta < 0$, in which $T^c$ also increases with decreasing $\beta$ while the onset of instability occurs mostly in the region near the outer cylinder. The third branch belongs to $\beta < \beta_{\max}$, where $T^c$ decreases with decreasing $\beta$ and the onset of instability is largely confined to a small region near the inner cylinder.

More specifically, as far as the onset flow pattern is concerned, the onset of instability is confined to the inner part of the gap for $\beta > 0$; for $\beta_{\max} < \beta < 0$, the region accommodating the onset of instability switches from the inner part to the outer part of the gap; for $\beta < \beta_{\max}$, the onset of instability is largely confined to a small region close to the inner cylinder. It is also found that as $T^c$ gets closer to the maximum value, the portion accommodating the onset flow becomes smaller, leaving a large part of the flow within the gap quiescent. That explains why the flow under this condition is of greater stability. In fact, near $\beta_{\max}$, both the stable and unstable regions are of approximately equal extent within the gap, which follows the argument of Chandrasekhar [26]. For $\beta < \beta_{\max}$, however, these two regions still share the gap spacing approximately equally, but the basic state is not at all the most stable.

### D. Nature of the neutral curves

There are two kinds of neutral curve for the present problem: one illustrates the variation of $T$ versus $a$ and the other accounts for the relation between $T$ and $m$. The neutral curve in the $T$-$a$ plane for the most unstable mode is mostly unimodal. As the change of instability mode occurs, the neutral curve consists of two branches, each of which accounts for a mode with different $m$, and accordingly, the neutral curve is bimodal. The bimodal instability apparently exists for the cases in which the change of mode accompanies a finite jump of $a^c$. This is evident by observing the neutral curves for $\eta = 0.7$ (Fig. 6), for instance, where the most unstable mode switches from $m = 2$ to $m = 0$ as $\beta$ changes from $-3.6$ to $-3.65$. In general, the bimodal stability becomes more significant as $\eta$ decreases.

With regard to the neutral curve in the $T$-$m$ plane, another interesting physical phenomenon is observed. The neutral curves for $\eta = 0.95$ are presented in Fig. 7. Each neutral curve accounts for the relation between $T^c/T_0^c$ and $m$, where $T_0^c$ is the critical Taylor number of $m = 0$. The points connected by a continuous curve are associated with the same value of $\beta$. From these neutral curves, one may find that, except for the cases of $\beta \sim \beta_{\max}$, the $T^c$ for the same $\beta$ but different $m$ are greatly different. Physically, it means, for a case with $\beta$ not lying in the neighborhood of $\beta_{\max}$, the most unstable mode is of relatively smallest stability compared with the other modes of different $m$. Nevertheless, as $\beta$ lies in the neighborhood of $\beta_{\max}$, the $T^c$ for the modes with different $m$ are of relatively smaller difference; moreover, we also note that the eigenfunctions of small perturbation velocity for these modes are similar, i.e., the threshold of the instability of different $m$ may occur in the same portion within the gap.

It is known that, if in a system there exist different modes of instability with similar stability criteria, such as $T^c$ and corresponding eigenfunctions, the interaction between these modes in the supercritical state ($T > T^c$) may be conducive to the bifurcations, the nonlinear interactions between the modes, and possible resonances of these modes [28]. For the present problem, this possibility lies in the neighborhood of $\beta_{\max}$. This inference is supported by the experimental observation of Mutabazi *et al.* [6,7]. Their experiments were conducted in a system consisting of two horizontal coaxial cylinders with a partially filled gap, corresponding to the case $\eta \approx 0.9$ and $\beta = -3$, which is close to $\beta_{\max} \approx -3.7$. They indicated that, in the su-

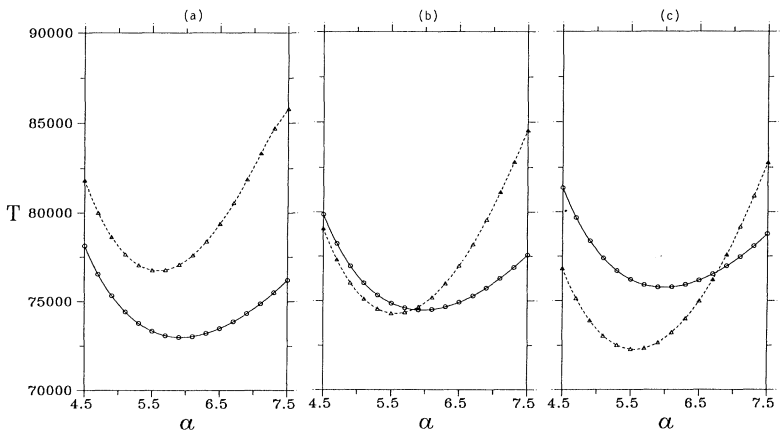


FIG. 6. Neutral curves of different modes for $\eta = 0.7$ and various $\beta$. —Δ—: $m = 0$; – – – ○ – – –: $m = 2$. (a) $\beta = -3.6$; (b) $\beta = -3.627$; (c) $\beta = -3.65$.

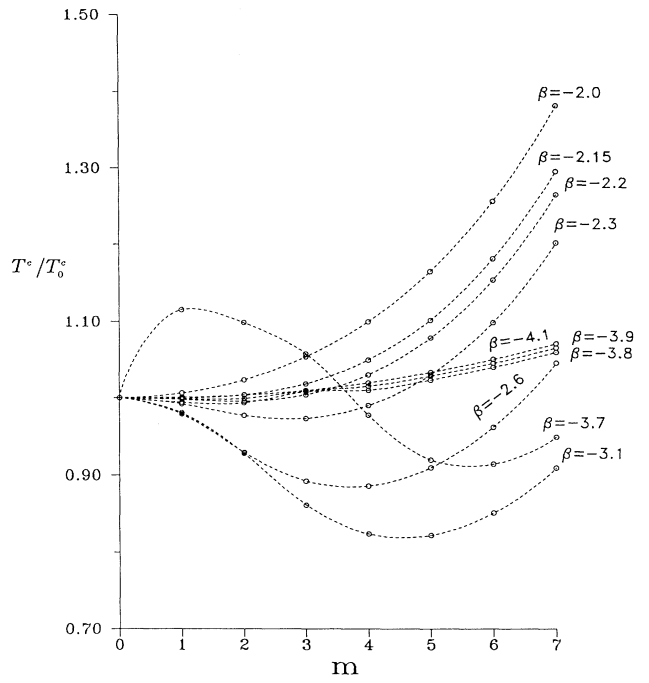


FIG. 7. Neutral curves in $(T^c/T_0^c)$-$m$ plane for various $\beta$ as $\eta=0.95$, where $T_0^c$ is the $T^c$ for $m=0$.

percritical regime, the instability forms a pattern of traveling waves, which are periodic in space and time. A periodic modulation of the instability modes was also reported.

### E. Comparison with previous results

In spite of the qualitative agreement between the experimental observation of Mutabazi *et al.* [6,7] and the inference made on the basis of present results, the quantitative comparison near the onset of instability is not so satisfactory. The quantitative comparison is made for the case $\mu=0$. The values of $\eta$ and $\beta$ corresponding to the system of Mutabazi *et al.* [6] are, respectively, 0.88 and $-3$. The present definition of the Taylor number $T$ is related to the $T_M$ of Mutabazi *et al.* [6] by $T\sim 2T_M^2$ as $\eta\approx 1$. According to this relation, the measured onset Taylor number is $T^c\approx 17\,300$, which is about half of the calculated value $T^c=36\,407$ of the present study. In addition, the measured frequency of Mutabazi *et al.* [6] is $\sigma\approx 20$, compared with the calculated value $\sigma=47.0933$. However, when comparing our results with the experimental results of Brewster and Nissan [5] (see Fig. 1 of DiPrima [10]), it is found that the calculated results of $\eta=0.95$ are in excellent agreement with those of Brewster and Nissan [5].

The difference between the results of the present calculation and the experimental data of Mutabazi *et al.* [6] is obviously due to the presence of the free surface within the gap. In such a partially-filled-gap system, according to both the measurement as well as the computation of Chen *et al.* [8] and to the analytical solution of Normand, Mutabazi, and Wesfreid [18], the basic flow consists of a core region, within which the flow is the fully developed Taylor-Dean flow described in Eq. (18), and two recirculation zones near free surfaces. Accordingly, the basic-state velocities of the present study and of the experimental investigations are different by the presence of free surfaces, which leads to quite distinct stability characteristics of these two basic flows. A satisfactory comparison may be obtained if the analysis is made based on the basic-state velocity shown in Normand, Mutabazi, and Wesfreid [18], in which the recirculation zones are considered. This attribution of the inconsistency between analytical and experimental results is supported by the experimental observation of Mutabazi *et al.* [6] that the threshold of instability occurs in the recirculation zone first and then in the core region. This may shed some light on the reason for the lower $T^c$ determined by their experiments.

In another analytical study, Mutabazi *et al.* [19] implemented a linear stability analysis for the case $\beta=-3$ and $\mu\geq 0$ with small-gap approximation $\eta\approx 1$. They found that the nonaxisymmetric modes prevail in the range $0.29\leq\mu\leq 0.61$, which is quite different from the results of Chen and Chang [21] that the nonaxisymmetric modes predominate in the system when $\mu\leq 0.35$. Particularly, for $\mu=0$, Mutabazi *et al.* [19] concluded that the most stable mode is axisymmetric ($m=0$) and the $T^c$ and $a^c$ are approximately 40 900 and 6.4, respectively. Although the values of $T^c$ and $a^c$ of the mode $m=0$ are consistent with previous results [10,14], Chen and Chang [21] nevertheless showed that for $\mu=0$ and $\beta=-3$, the onset of flow instability is nonaxisymmetric with $m=4$ and $T^c\approx 33\,900$ and $a^c\approx 4.7$, which is also confirmed by the present study with $\eta=0.95$ (Table II). The reason for the discrepancy between Mutabazi *et al.* [19] and Chen and Chang [21], as well as the present study, is not yet clear.

## IV. CONCLUDING REMARKS

We have implemented a three-dimensional linear stability analysis for the Taylor-Dean flow within an annulus with arbitrary gap spacing. In the parametric study covering wide ranges of $\eta$ and $\beta$, two major parameters determining the basic flow, several conclusions are reached for the stability characteristics: (a) A three-dimensional consideration for the stability analysis of the Taylor-Dean flow is essential since, for a wide variety of basic states, the nonaxisymmetric instability prevails. (b) Nonaxisymmetric modes predominate in the system when $0.25\leq\eta\leq 1$ and $-4\leq\beta\leq -2.2$, in which the azimuthal wave number varies $m$ from 0 to 5. (c) The most stable state occurs in two situations: one when a nonaxisymmetric mode is preparing to switch into an axisymmetric mode as $\beta$ decreases, the other when a nonaxisymmetric mode changes both its traveling-wave direction as well as its azimuthal wavelength as $\beta$ varies. (d) A most stable state is always associated with the smallest critical axial wavelength, where the onset of instability is largely confined to a small portion of the gap. (e) The azimuthal wave number $m$ decreases as $\eta$ increases. It means that a larger gap width accommodates a nonaxisymmetric mode of larger azimuthal wavelength. (f) Due to the similarity

in terms of $T^c$ and associated eigenfunctions holding for different instability modes when $\beta \sim \beta_{max}$, some sort of nonlinear interaction between these modes in a supercritical regime may occur in the Taylor-Dean flow, as observed in the experiments of Mutabazi *et al.* [6,7].


## ACKNOWLEDGMENT

The financial support for this work from the National Science Council through Grant No. NSC 81-0401-E-002-503 is gratefully acknowledged.



[1] G. I. Taylor, Philos. Trans. R. Soc. London A **223**, 289 (1923).
[2] W. R. Dean, Proc. R. Soc. London A **121**, 402 (1928).
[3] A. Y. Komada, Kawasaki Steel Tech. Rep. **8**, 17 (1983).
[4] M. Nabatame, Nippon Kokan Tech. Rep. Overseas **40**, 9 (1984).
[5] D. B. Brewster and A. H. Nissan, Chem. Eng. Sci. **7**, 215 (1958).
[6] I. Mutabazi, J. J. Hegseth, C. D. Andereck, and J. E. Wesfreid, Phys. Rev. A **38**, 4752 (1988).
[7] I. Mutabazi, J. J. Hegseth, C. D. Andereck, and J. E. Wesfreid, Phys. Rev. Lett. **64**, 1729 (1990).
[8] K. S. Chen, A. C. Ku, T. M. Chan, and S. Z. Yang, J. Fluid Mech. **213**, 149 (1990).
[9] D. B. Brewster, P. Grosberg, and A. H. Nissan, Proc. R. Soc. London A **251**, 76 (1959).
[10] R. C. DiPrima, J. Fluid Mech. **6**, 462 (1959).
[11] B. Meister, Z. Angew, Math. Phys. **13**, 83 (1964).
[12] E. M. Sparrow and S. H. Lin, Phys. Fluids **8**, 229 (1965).
[13] U. H. Kruzweg, Z. Angew, Math. Phys. **14**, 380 (1963).
[14] T. H. Hughes and W. H. Reid, Z. Angew. Math. Phys. **15**, 573 (1964).
[15] D. C. Raney and T. S. Chang, Z. Angew. Math. Phys. **22**, 680 (1971).
[16] B. J. Kachoyan, Z. Angew. Math. Phys. **38**, 905 (1987).
[17] J. H. Vohr, Trans. ASME F **11**, 285 (1968).
[18] C. Normand, I. Mutabazi, and J. E. Wesfreid, Eur. J. Mech. B **10**, 335 (1991).
[19] I. Mutabazi, C. Normand, H. Peerhossainti, and J. E. Wesfreid, Phys. Rev. A **39**, 763 (1989).
[20] I. Mutabazi, J. E. Wesfreid, J. J. Hegseth, and C. D. Andereck, Eur. J. Mech. B **10**, 239 (1991).
[21] F. Chen and M. H. Chang, J. Fluid Mech. **243**, 443 (1992).
[22] E. R. Krueger, A. Gross, and R. C. DiPrima, J. Fluid Mech. **24**, 521 (1966).
[23] R. C. DiPrima, Q. Appl. Math. **13**, 55 (1955).
[24] D. L. Harris and W. H. Reid, J. Fluid Mech. **20**, 95 (1964).
[25] E. M. Sparrow, W. D. Munro, and V. K. Jonsson, J. Fluid Mech. **20**, 35 (1964).
[26] S. Chandrasekhar, *Hydrodynamic and Hydromagnetic Stability* (Clarendon, Oxford, 1961).
[27] X. Rayleigh, Proc. R. Soc. London A **93**, 148 (1916).
[28] R. C. DiPrima, and J. Sijbrand, in *Stability in the Mechanics of Continua,* edited by F. H. Schroeder (Springer, Berlin, 1982), p. 383.